
Volume 14, Issue 1, 142403 (1-14)

Iranian Journal of Catalysis (IJC)

https://doi.org/10.57647/j.ijc.2024.1401.03

# $G/In_2O_3$ nanocatalyst modified pencil graphite electrode for the electrochemical detection of Favipiravir

Shaila Sanjeevagol[1], Jayappa Manjanna[1]*, Rudrappa Chaithra[2]

[1]*Department of Chemistry, Rani Channamma University, Belagavi, Karnataka, India.*
[2]*Department of Biochemistry, Kuvempu University, Shankaraghatta, Shimoga-Dist., Karnataka, India.*

*__Corresponding author:__ jmanjanna@gmail.com

**Original Research**

Received:
4 September 2023
Revised:
4 December 2023
Accepted:
10 January 2024
Published online:
29 March 2024

© The Author(s) 2024

**Abstract:**

Favipiravir (FVP) was one of the promising medications for the treatment of Covid-19 patients. There are limited studies on the electrochemical performance of FVP. Hence it is interesting to study the electrochemical detection of FVP by cyclic voltammetry (CV), differential pulse voltammetry (DPV) and chronoamperometry. The $G/In_2O_3$ nanocatalyst was prepared by precipitation method and applied on the pencil graphite electrode by drop-cast method, the electrode represented here as $G/In_2O_3$/MPGE and used as a working electrode for the detection of FVP in a pH 7 Britton Robinson (BR) buffer. The oxidation signal was seen in the region of 1.0 to 1.23 V. The predicted linear range is between 0.7 to 4.9 $\mu$M. The corresponding limit of detection (LOD) and limit of quantification (LOQ) were found for pure drugs at 0.28 $\mu$M and 0.93 $\mu$M, whereas for samples in commercial tablets, it is 0.23 and 0.79 $\mu$M. The same in the presence of urine medium is 0.30 and 106 $\mu$M, respectively. The developed $G/In_2O_3$/MPGE offers good detection, selectivity, reasonable stability, and reproducibility to detect FVP in pure drug, tablet form, and in the presence of urine.

**Keywords:** Favipiravir, COVID-19; Modified pencil graphite electrode; $G/In_2O_3$ nanocatalyst; Voltammetry

## 1. Introduction

Severe acute respiratory syndrome coronavirus 2 (SARS-CoV-2) is a single-stranded RNA virus that first surfaced in Wuhan, China, in December 2019. It is closely related to coronaviruses that resemble SARS originated from bats [1, 2]. The WHO announced that COVID-19 is a worldwide emergency on March 11, 2020 [3]. Since then, millions of human beings have become infected as a result of the sharp spread of viruses globally. Thus, the COVID-19 causing agent is SARS-CoV-2. Fever, dry cough, breathing trouble, muscle or joint uneasiness, headache or dizziness, a reduced ability to odor and taste, diarrhea, and nausea are typical signs or signs of COVID-19. Acute respiratory distress syndrome, which causes certain patients to have a lack of oxygen in their blood, can ultimately lead to breathing problems. Multi-organ injury is brought by the virus infection and the massive production of cytokines (cytokine storm). Inflammatory symptoms and additional infections caused 28% of the deaths of Covid-19 patients [4, 5]. Chemically, favipiravir (FVP) is 6-fluoro-3-hydroxy-2-pyrazinecarboxamide ($C_5H_4FN_3O_2$), which is also known as T-705. It is effective against a variety of viruses, which are pathogenic across a broad range of antiviral agents [6]. In Japan, Fujifilm Toyama (a pharmaceutical company) produced FVP. It particularly suppresses the enzyme, RNA-dependent RNA polymerase (RdRP) [7–9]. FVP was sold as an additional treatment during the second wave of coronaviruses and as strains of influenza in China (Favilavir) and Japan (Avigan) [10]. Also, FVP was recommended to suppress RdRP viruses like Ebola, chikungunya, yellow fever, norovirus and enterovirus [11]. FVP successfully reduces the SARS-CoV-2 infection by obstructing its RNA synthesis [12]. Following the deadly Ebola virus outbreak in West Africa in 2014, it was suppressed by FVP treatment [13]. Early in the global epidemic research, investigations were started to evaluate the effectiveness of HCQ and FVP in curing COVID-19 patients. Some possible medicines listed worldwide in multiple formulations for the treatment of COVID-19 include the antimalarial drug HCQ, the antivi-

ral pharmaceuticals like FVP, lopinavir/ ritonavir, darunavir, remdesivir and oseltamivir [2, 14].

Several analytical methods such as high-performance liquid chromatography (HPLC) [15], colorimetric analysis method (CAM) [16], thin layer chromatography (TLC) [17], liquid chromatography-tandem mass spectrometry (LC-MS) [18] are known for the detection of FVP in medicinal products and biological fluids. Electrochemical techniques have advantages over these conventional analytical methods in terms of its simplicity, rapid detection, redox behavior of analytes, flexibility, lower LOD, etc. It provides a physicochemical characteristics, significant catalytic efficiency through the modified working electrode, high sensitivity, stability and it is inexpensive [19–21].

Electrochemical sensors are widely used to assess trace levels of pharmaceuticals and other analytes from medicinal, biological, and ecological materials [22]. To detect analytes through a bare electrode is challenging due to the slow transfer of electrons, and hence electrochemical sensors must be improved with suitable materials to increase their analytical efficiency. The enhanced surface area by employing a modified electrode helps to detect the analyte [23]. Furthermore, the improved interfacial adsorption characteristics of carbon nanocomposites are advantageous [24]. Thus, we used graphene as conducting materials with indium oxide nanocatalyst as the electrochemical sensor.

Graphene (G) has a flat monolayer with $sp^2$ hybridized carbon atoms and a closely packed two-dimensional hexagonal lattice with a distinctive nanostructure [25]. It is widely used to modify different working electrodes for the detection of Ciprofloxacin [26], Chloramphenicol [27] and DNA sensors, etc. [28]. $In_2O_3$ is an n-type semiconductor and is extensively used in semiconducting devices due to its wide bandgap (around 3.65 eV). $In_2O_3$ nanostructures include nanocones, nano bouquets, nanotowers, hollow microspheres, hollow nanofibers, urchin-like $In_2O_3$, etc. [29–32]. These materials/composites are used as biosensors and gas sensors. Novel urchin-like $In_2O_3$–chitosan-modified electrodes are used for electrochemical detection of glucose oxidase and biosensing [33]. On the other hand, $In_2O_3$/graphene heterostructure showed hydrogen gas sensing properties [34]. The nanocatalysts are utilized as surface modifiers in electrochemical sensors. The $In_2O_3$ nanostructures/composites are used as electrocatalysts for the detection of ethanol [35], formaldehyde [36], ammonia [30], and uric acid [37].

The combination of $In_2O_3$ with G can lead to significantly improved catalytic activity. Graphene provides a high surface area and excellent electronic conductivity, which can facilitate the efficient transport of charge carriers, leading to enhanced catalytic performance. The characteristic features of G/$In_2O_3$ include enhanced surface area and active sites towards the electrochemical detection of FVP. The low levels of FVP in real samples could be efficiently detected here by using G/$In_2O_3$/MPGE in CV and DPV techniques. The different materials used for the detection of FVP by various techniques, including CV and DPV, are listed in Table 1.

## 2. Experimental

### 2.1 Chemicals and apparatus

The FVP (Hetero Healthcare Limited, Hyderabad) tablets were purchased from a local pharmacy and used as an analyte (contains 200 mg of FVP per tablet); SEUTIC Labs PVT LTD supplied the original form of FVP. The G/$In_2O_3$ nanocatalyst was prepared by using indium chloride, ammonia, graphene and ethanol. Graphene was supplied by Anderlab Technologies Pvt. Ltd. Briton-Robinson buffer (BR buffer, pH 7) and was prepared by using equimolar (0.1 M) solutions of boric acid, acetic acid, and phosphoric acid. An Equimolar (5 mM) mixture of potassium ferricyanide and ferrocyanide solution was prepared in 0.1 M KCl as a standard analyte for optimizing the material for the working electrode. All the experiments were done with freshly prepared solutions using analytical-grade chemicals in distilled water.

TG/DSC plot was obtained using a TA instrument SDT Model 650, and FT-IR spectra was taken using a Thermo Scientific Nicolet iS5 analyzer by KBr pellet technique. Field emission scanning electron microscopy (FE-SEM, model JEOL JSM-7100F) was used to record the microstructural images of the $In_2O_3$ nanocatalyst. Shimadzu's UV-1800 spectrophotometer was used for recording the UV-visible spectra. The electrochemical analyses were performed in the three-electrode setup using Metrohm Autolab PGSTAT204.

### 2.2 Synthesis of $In_2O_3$ and G/$In_2O_3$ nanocatalyst

Graphene (G, 0.0221 g) was added to $6.3 \times 10^{-3}$ M $InCl_3$ (i.e., 0.1392 g in 100 mL) solution kept in stirred condition. Then $NH_4OH$ was added drop by drop till pH 9 to form a jelly precipitation. It was filtered and washed thoroughly with distilled water and ethanol. It was dried in an oven at 80 °C for 5 h and then at 400 °C for 15 h in a muffle furnace to obtain the final product, G/$In_2O_3$ nanocatalyst (having 15 wt.% of G and 85 wt.% of $In_2O_3$. The same procedure has been applied for the preparation of $In_2O_3$ in the absence of graphene [38].

### 2.3 Fabrication of pencil graphite-electrode

A pencil graphite electrode was fabricated by inserting pencil graphite (Sigma 4 mm diameter) into a hollow Teflon tube and making electrical contact with a copper wire. The pencil graphite electrode surface was polished to a mirror-shiny finish with the aid of a PK-3 electrode polishing kit. It was cleaned with distilled water by ultrasonication and then dried. A 10 $\mu$L of G/$In_2O_3$ nanocatalyst (10 mg/mL) suspension was drop cast on this pencil graphite electrode surface and dried for 5 h at ambient conditions. This modified pencil graphite electrode, abbreviated as G/$In_2O_3$/MPGE, served as the working electrode here.

### 2.4 Sample preparation

A 1.5 g finely powdered FVP sample was dissolved in 10 mL of distilled water and sonicated for 30 minutes to ensure a complete dispersion. Then, it was filtered using through 0.4 $\mu$m pore size membrane filter paper to obtain a stock solution of 0.07 M of FVP. Different concentrations (0.7 to

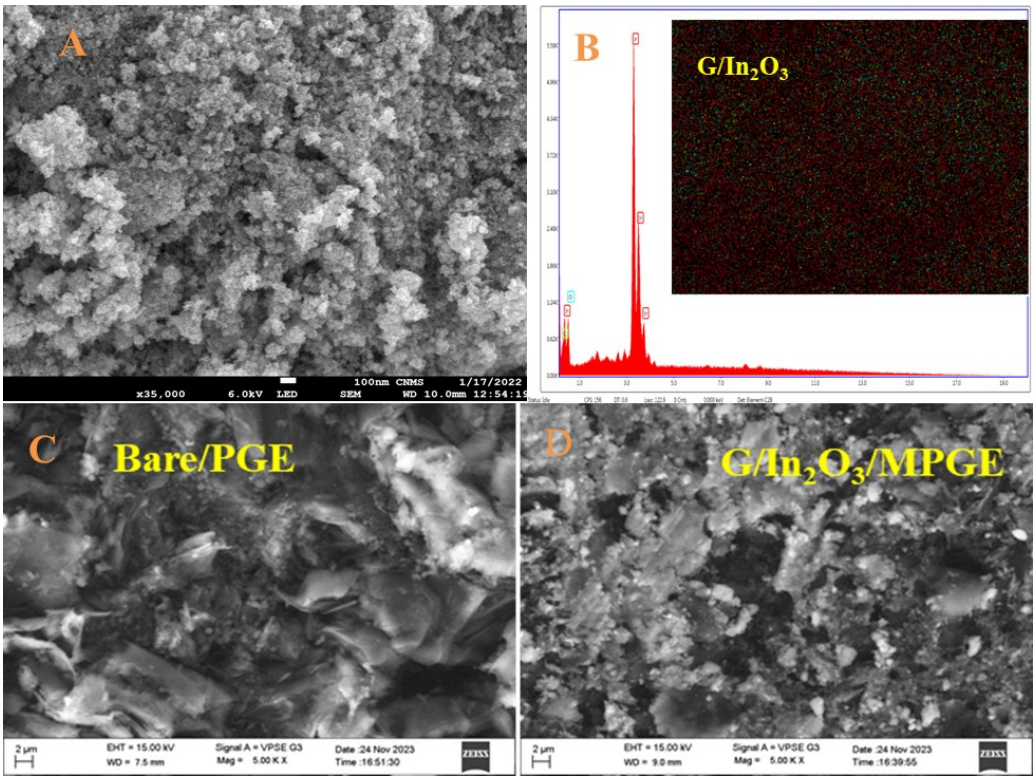


**Figure 1.** (A) FE-SEM, (B) EDX spectra of G/$In_2O_3$ (inset is the elemental mapping), (C) SEM image of bare PGE and (D) G/$In_2O_3$/MPGE.

4.9 $\mu$m ) were prepared from this stock solution, and added to 0.1 M BR buffer and analyzed using cyclic voltammetry (CV) and differential pulse voltammetry (DPV) techniques. The BR buffer capacity is relatively high, which means it can resist rapid changes in pH, providing stability to the electrochemical system during the experiment and good detection for FVP [39, 40]. The physiological pH 7 was chosen here because most of the pharmaceutical and biomolecules react around neutral pH 7 [41, 42]. The other tablets were also used here in the same way to obtain HCQ ($1.89 \times 10^{-4}$ M), Paracetamol ($2.38 \times 10^{-4}$ M) and Acivir ($1.661 \times 10^{-4}$ M) drug samples and studied here as co-administered drugs with FVP.

## 3. Results and discussion

### 3.1 XRD characterization

Fig. S1 shows the powder XRD pattern of G/$In_2O_3$ nanocatalyst and its Rietveld refinement using Match! Supporting full-proof software is shown in Fig. S2. This pattern could be indexed to the body-centered cubic bixbyite structure for $In_2O_3$ with a lattice constant of a = b = c = 10.117 Å having a space group (I a-3) according to the crystallography open database (COD card no. 96-231-0010) [34]. The $In_2O_3$ phase is highly crystalline, whereas the G is amorphous and present in a small portion (15 wt.%); the XRD peak expected for G (002) around $2\theta = 21°$ is not seen here. The crystallite size (D) was calculated by Scherer equation: $D = 0.9\lambda/\beta\cos\theta$ where $\lambda = 0.154$ nm, wavelength of Cu $K_\alpha$ line, and $\beta$ is the FWHM in radians of the 100% peak (222) in the XRD pattern. Accordingly, D of G/$In_2O_3$ was found to be around 10 nm.

### 3.2 FTIR analysis

Fig. S3 shows the FTIR spectra of G and G/$In_2O_3$. The peak around 3435 $cm^{-1}$ is due to the O-H stretching vibrations of adsorbed water molecules. The carboxyl C=O stretching band around 1637 $cm^{-1}$ and the O-H bending vibration around 1382 $cm^{-1}$ are seen here. The stretching and bending vibrations of In-O bond in G/$In_2O_3$ are observed around 570 and 460 $cm^{-1}$ [43, 44].

### 3.3 FESEM and EDX analysis

Fig. 1(A) shows the SEM image of G/$In_2O_3$ consisting of polydisperse particles and/or irregular morphology. Fig. 1(B) is the EDX spectra, and the inset shows the elemental mapping exhibiting a homogenous distribution of $In_2O_3$ on the surface of the G. EDX analysis here was intended to check the expected elements and to make sure that no impurity is present. Fig. 1(C) and Fig. 1(D) show the SEM images of bare (PGE) and G/$In_2O_3$/MPGE. The morphology of electrocatalysts greatly influences the sensing performance of the analytes [45, 46]. The G/$In_2O_3$/MPGE shows a relatively smooth surface, unlike the bare electrode surface.

### 3.4 TG-DSC characterization

The thermal analysis (TG-DSC) of the G/$In_2O_3$ nanocatalyst is depicted in Fig. S4. The first step weight loss is about 3% when heated from ambient temperature to 10 °C due to the removal of surface absorbed moisture. The DSC curve has an endothermic high point at 146 °C, and there-

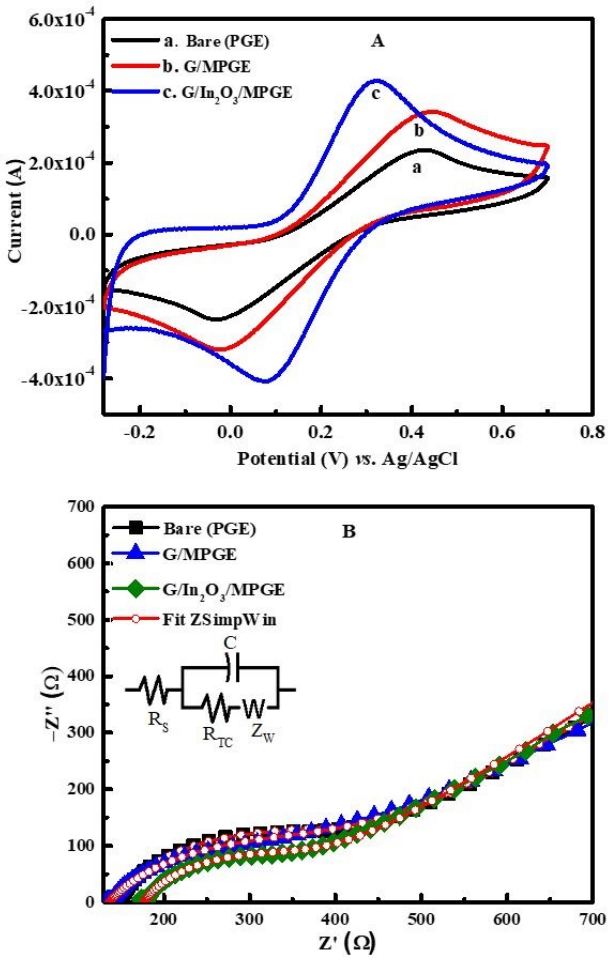


**Figure 2.** (A) CV curves at a scan rate of 0.1 $Vs^{-1}$ for 5 mM $[Fe(CN)_6]^{3-/4-}$ in 0.1 M KCl solution using bare, G/MPGE and $G/In_2O_3$MPGE, (B) Nyquist plots for these three electrodes.

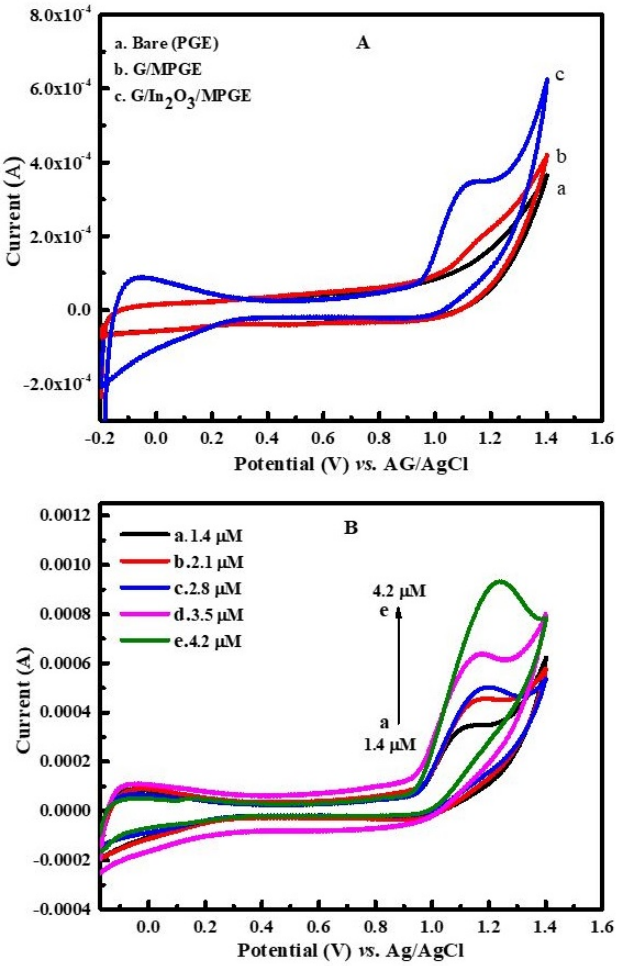


**Figure 3.** (A) CV curves for 1.4 $\mu$M FVP using bare, G/MPGE and $G/In_2O_3$/MPGE in BR buffer at a scan rate of 0.1 $Vs^{-1}$, (B) 1.4 to 4.2 $\mu$M FVP.

after, no endothermic or exothermic peaks are seen. An overall weight loss of about 5.8% was seen when heated up to 600 °C. The gradual weight loss of about 3% after heating above 146 °C is ascribed to the removal of surface functional groups such as -OH (possible impurities) to produce thermally stable $G/In_2O_3$ [47]. The UV-Vis spectrum of FVP is shown in Fig. S5. In the UV region, there are two absorption bands at 221 and 325 nm, which is corroborated by previous reports [48, 49].

### 3.5 Electrochemical behavior of $G/In_2O_3$/MPGE

Fig. 2(A) shows the CV of 5 mM $[Fe(CN)_6]^{3-/4-}$ in 0.1 M KCl at a scan rate of 100 $mVs^{-1}$, and it is clear that $G/In_2O_3$ nanocatalyst is superior when compared to the bare electrode and graphene-modified pencil graphite electrode (G/MPGE). The shift in peak potential suggests that the $In_2O_3$ nanocatalyst lowers the activation energy required for the electrode reaction, leading to improved electron transfer kinetics. The $G/In_2O_3$/MPGE showed increased peak current and enhanced surface area due to an increase in electron transfer reactions. The MPGE surface area values for the bare PGE, G/MPGE, and $G/In_2O_3$/MPGE are 0.039, 0.042, and 0.048 $cm^2$, respectively.

The surface area of the electrode was calculated by the Randles-Sevcik equation, $Ipa = (2.69 \times 10^5)AD^{1/2}n^{3/2}v^{1/2}C$ where $C$ is the concentration (mol/$cm^3$), $D$ is the diffusion coefficient ($cm^2$/s), $A$ is the electrode surface area ($cm^2$), $v$ is the scan rate (V/s), and $n$ is the number of electrons transferred. The peak current and the concentration, as well as the square root of the scan rate, are directly correlated, according to the above equation.

Fig. 2(B) displays the Nyquist plots recorded to compare the charge transfer capacity of bare, G/MPGE, and $G/In_2O_3$/MPGE in 5 mM $[Fe(CN)_6]^{3-/4-}$ with 0.1 M KCl. The obtained Nyquist plots depicted a small semi-circular arc with a Warburg-type line. This smaller semicircle arc for $G/In_2O_3$/MPGE indicates the high charge transfer and increased kinetics. The data was fitted to the $[R_S(C(R_{CT}Z_W))]$ circuit model and obtained $R_S$ (resistance, 181.1 Ω), $C$ (capacitance, $1.232 \times 10^{-5}$ F), and $R_{CT}$ (charge transfer resistance, 147.6 Ω), respectively. The $R_{CT}$ measuring the bulk diffusion is connected to the impedance, $Z_W(1.575 \times 10^{-3}\ \Omega)$, which denotes Warburg-type impedance, i.e., $R_{CT}$ and $Z_W$ are parallel to the capacitance. The $R_{CT}$ values for bare, G/MPGE

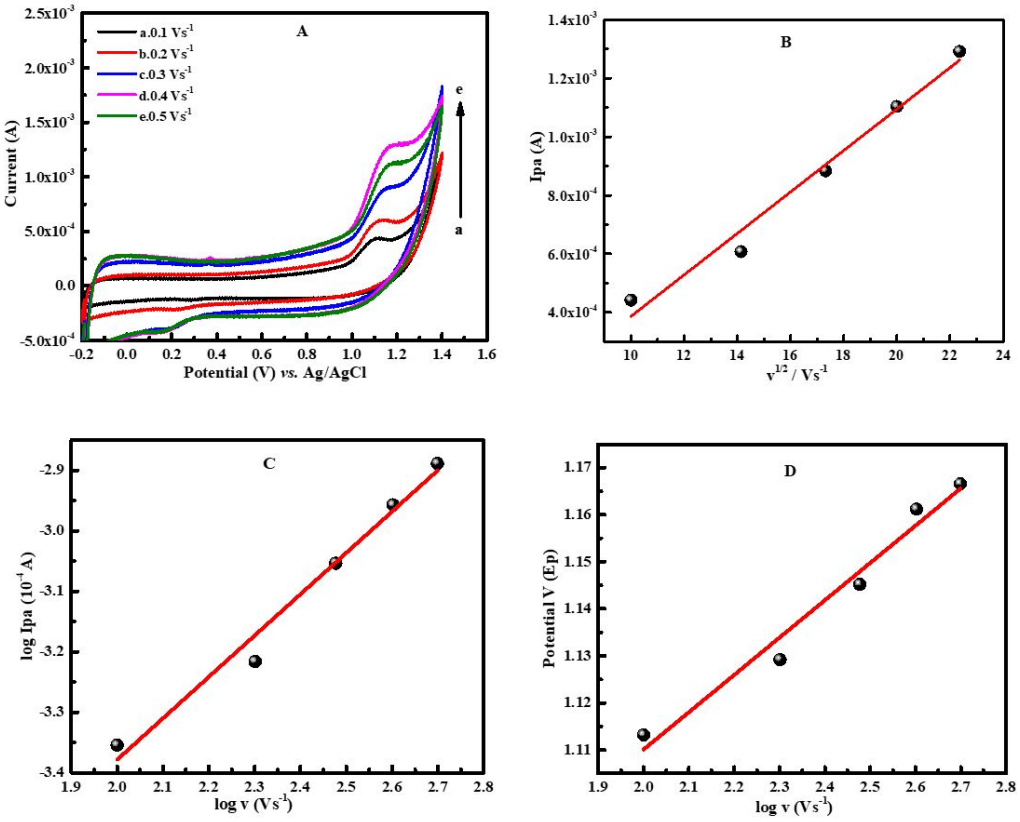


**Figure 4.** (A) CVs of 1 mM FVP at various scan rate (0.1 to 0.5 $mVs^{-1}$), (B) plot of Ipa *vs.* $v^{1/2}$, (C) logIpa *vs.* $\log \nu$ and (D) $Ep$ *vs.* $\log \nu$.

and G/$In_2O_3$/MPGE are 206.2 Ω, 174.1 Ω and 147.6 Ω, respectively. Thus, G/$In_2O_3$/MPGE has shown better electronic charge transfer and a decrease in $R_{CT}$, thereby giving high electronic conductivity and large surface area compared to bare and G/MPGE. These results obtained here are in good agreement with the reported values [50]. The heterogeneous electron transfer rate constant $k^\circ$ for electronic charge transfer can be calculated using $R_{CT}$ values using the equation given below.

$$k^\circ = \frac{RT}{F^2 R_{CT} A C}$$

where $R$ is the universal gas constant (8.3145 J $mol^{-1}$ $K^{-1}$), $T$ is the thermodynamic temperature (298.15 K), $F$ is Faraday's constant (96485 C $mol^{-1}$), $A$ is the geometrical surface area of the electrode (0.05 $cm^2$), and $C$ is the concentration of the electrolyte (5 mM). The $k^\circ$ obtained here are $0.982 \times 10^{-8}$, $1.159 \times 10^{-8}$ and $1.372 \times 10^{-8}$ $cm^2$ $s^{-1}$ for the bare, G/MPGE and G/$In_2O_3$/MPGE, respectively. Thus, G/$In_2O_3$/MPGE exhibits a maximum value of $R_{CT}$, which represents the high rate of electronic transfer over the electrode surface [51, 52].

### 3.6 Electrochemical oxidation of FVP

The cyclic voltammetry (CV) method was used to assess the electrochemical oxidation of FVP. Fig. 3(A) shows various catalytic behaviors of the bare electrode, G/MPGE, and G/$In_2O_3$/MPGE towards FVP. There was no significant response by the bare electrode for 1.4 $\mu$M FVP, whereas G/MPGE produced a considerably higher anodic peak current. This indicates the presence of additional active sites for electron transport. However, G/$In_2O_3$/MPGE showed a more effective anodic peak current for FVP detection. Compared to the bare electrode, G/$In_2O_3$/MPGE exhibited higher conductivity along with an efficient surface. It implies that oxidation is an irreversible process [53]. Fig. 3(B) shows the CV for 1.4 to 4.2 $\mu$m FVP, and the peak current was maximum for G/$In_2O_3$/MPGE due to higher electro-catalytic activity [54].

Fig. 4(A) shows the CV of 1.4 $\mu$M FVP at different scan rate (0.1 and 0.5 $Vs^{-1}$) using G/$In_2O_3$/MPGE at pH 7 BR buffer. The Ipa increased linearly with the scan rate. According to Fig. 4(B), the electrocatalytic process is regulated by FVP diffusion to the electrode surface, as seen by the linear plot of Ipa *vs.* $v^{1/2}$ with Ipa($\mu$A) = 7.0809 ($v^{1/2}$, V/s) - 3.2111; $R^2 = 0.97$ . As the scan rate increased, the normalized peak current decreased [55, 56]. Fig. 4(C) shows the regression plot of log Ipa *vs.* log v. The linear relationship, logIpa ($\mu$A) = 0.6839 ($\log \nu$, V/s) - 4.7463; $R^2 = 0.98$ indicate the diffusion control mechanism. The results of Fig. 4(D) indicated a linear correlation between peak potential ($Ep$) and log $\nu$: $Ep$ (V) = 0.0793 ($\log \nu$) - 0.9513; $R^2 = 0.97$. For an irreversible reaction, the Laviron equation demonstrates the correlation between the anodic peak potential ($Epa$) and scan rate.

$$Ep = E^\circ + (2.303RT/\alpha nF)\log(RTK^\circ/\alpha nF) + (2.303RT/\alpha nF)\log \nu$$

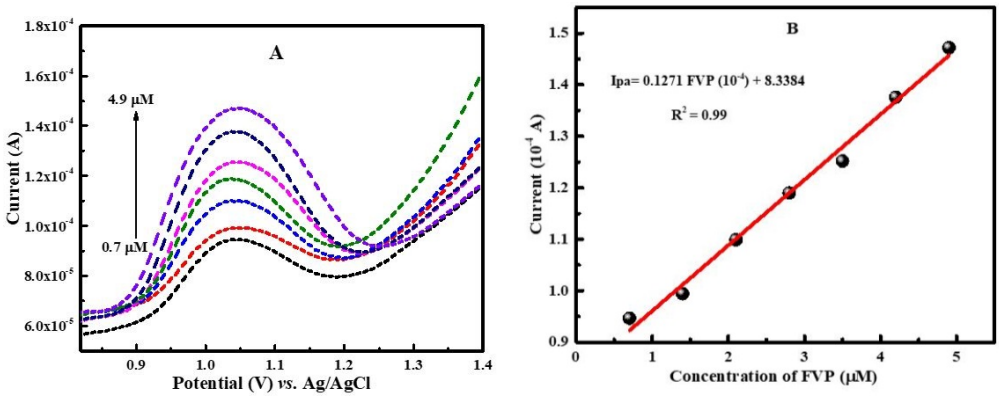


**Figure 5.** (A) DPV and (B) calibration plot for pure FVP (0.7 to 4.9 $\mu$M).

The number of electrons transmitted ($n$) and the electron transfer coefficient ($\alpha$) were determined. The formal potential is represented by $E^\circ$ in the Laviron equation, $F = 96.480$ C mol$^{-1}$, $\nu$ represents the potential scan rate, and $k^\circ$ is the standard heterogeneous rate constant. All coefficients were calculated using the slope of the $Ep$ vs. $\log \nu$ plot, $\alpha = 0.5$ and $n = 1.49$ (i.e., $\sim 1$) shown in Fig. 5(C). Furthermore, if the value of $E^\circ$ is known, the value of $k^\circ$ can be calculated from the intercept of Fig. 5(C). The Laviron equation yielded $k^\circ = 10.6071$ and $E^\circ = 1.1325$ [57, 58].

Fig, 5(A) shows the differential pulse voltammetry (DPV) plots for pure FVP (0.7 to 4.9 $\mu$M) using G/$In_2O_3$/MPGE at a scan rate of 0.1 mV/s. A linear increase in the peak current was seen with increasing [FVP], as shown in Fig. 5(B) with a linear equation, Ipa $= 0.1271\text{FVP} \times 10^{-4} + 8.3384 (R^2 = 0.99)$. The Limit of detection (LOD = 3 SD/S) and limit of quantification (LOQ = 10 SD/S) were determined to be 0.28 $\mu$M and 0.93 $\mu$M, respectively, where SD is the standard deviation of three observations made from the signal acquired from the blank (blank readings of DPV curve in the presence of BR buffer) and $S$ (= 0.1271) is the slope of its calibrate curve. The 3 is a result for 90% confidence level in the distinction between the observed signal and the blank [59].

For commercially available FVP tablets, the DPV was recorded using G/$In_2O_3$/MPGE as depicted in Fig. 6. The peak current and FVP concentrations are linearly related with Ipa $= 0.1657\text{FVP} \times 10^{-4} + 7.9911$ ($R^2 = 0.99$). Accordingly, LOD = 0.23 $\mu$M and LOQ = 0.79 $\mu$M are obtained.

After successful detection of pure FVP and tablet form, the detection was done for FVP in the presence of a urine sample (prepared by adding 2 mL of healthy adult's urine sample to 8 mL of 0.1 M BR buffer in the presence of 10 $\mu$M of 0.7 to 4.9 $\mu$M of pure FVP). The urine sample was added without any pre-treatment, and the pH of the BR buffer remained the same even after mixing with a urine sample and FVP. Fig. 7(A) shows the DPV for the above solutions using G/$In_2O_3$/MPGE, and Fig. 7(B) shows the calibration curve, Ipa vs. [FVP] which is linearly related with Ipa $= 0.1269\text{FVP} \times 10^{-4} + 8.3441$ ($R^2 = 0.99$). The observed LOD was 0.30 $\mu$M whereas LOQ was 106 $\mu$M. Thus, FVP could be detected in the presence of biological fluids such as urine [39]. FVP is oxidized within the potential range of 1.05 V to 1.23 V as seen from both the CV and DPV peaks. As there was no reversible peak in CV, the process of oxidation is considered to be irreversible. The calibration curves (Fig. 6(B) and Fig. 7(B)) for the sample in the presence and absence of urine have marginally varied. Table 2 shows the analysis of FVP by DPV in tablet and urine samples. It is clear that more than 95% of the detection efficiency (recovery) is achieved here for 3 to 5 $\mu$M of FVP.

The proposed reaction with a mechanism for the electro-

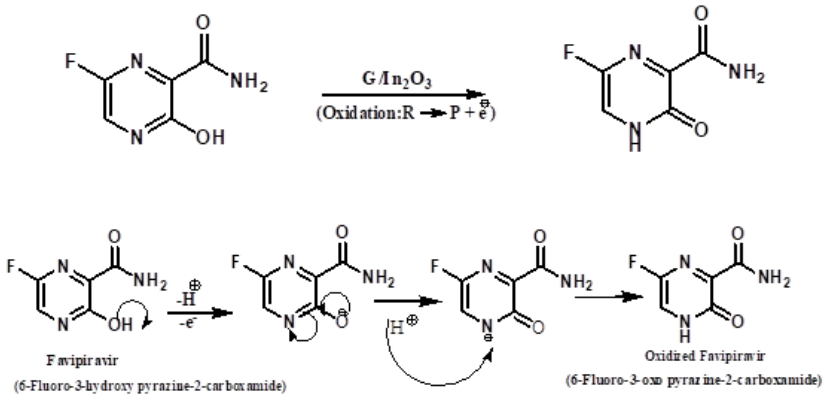


**Scheme1.** Electrochemical oxidation of FVP on the surface of G/$In_2O_3$/MPGE.

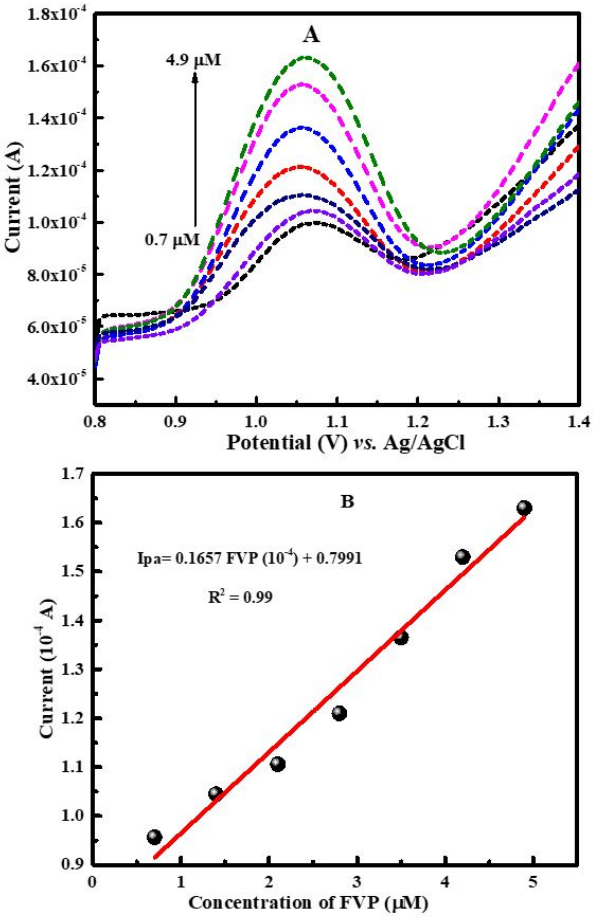


**Figure 6.** (A) DPV and (B) calibration plot for FVP tablet (0.7 to 4.9 $\mu$M).

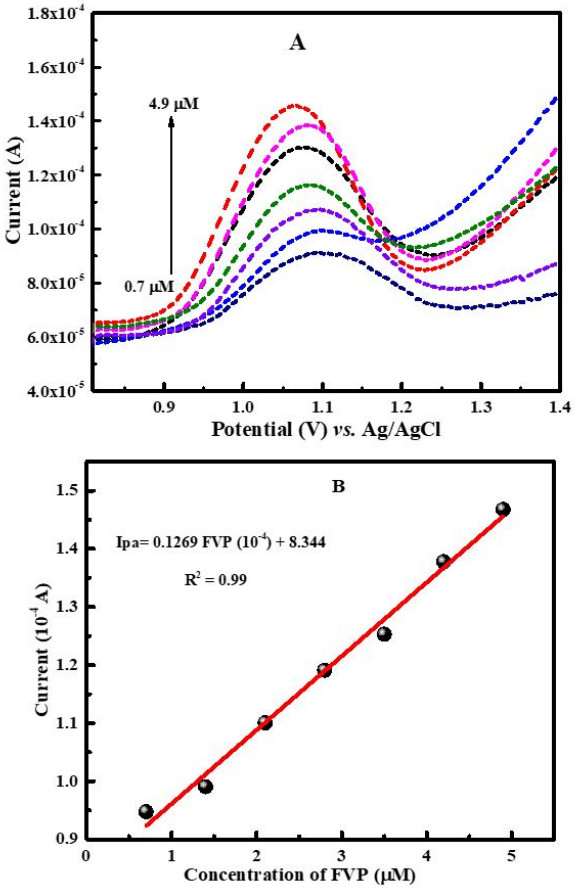


**Figure 7.** (A) DPV of FVP (0.7 to 4.9 $\mu$M in presence of human urine) in 0.1 M BR buffer (B) its calibration plot.

chemical (CV/DPV) oxidation of FVP is illustrated in Scheme 1. The oxidation of the FVP molecule involves the deprotonation of the hydroxyl group. At the same time, the oxygen becomes negatively charged, and then the amine group is protonated to form a stable amino group. Thus, the 3 hydroxyl group is converted into a carbonyl group to form 6-Fluoro-3-oxo-pyrazine-2-carboxamide (product). G/$In_2O_3$ nanocatalyst present on the electrode surface enables lowering of activation energy (i.e., accelerate the kinetics of electron transfer due to enhanced active sites) needed for oxidation reaction, Reactant $\rightarrow$ Product $+ e^-$

### 3.7 Detection of FVP by DPV in the presence of interfering drugs

The electro-analytical performance of G/$In_2O_3$/MPGE was tested for specificity by detecting FVP in a solution of the antiviral medication hydroxychloroquine (HCQ), which was recently utilized to treat COVID-19 patients. Simultaneously, antiviral drugs paracetamol (PAR) and acivir were also detectable with FVP. However, lopinavir and ivermectin drugs could not be detected along with FVP. Fig. 8(A) shows the concurrent detection of co-administered drugs, FVP ($2 \times 10^{-5}$ M) and HCQ ($1.8 \times 10^{-4}$ M). HCQ

**Table 1.** FVP detection by different methods.

| Methods | Linearity Range | LOD | Ref. |
|---|---|---|---|
| HPLC & UC | 10-100 $\mu$L | 1.20 $\mu$g/mL | [15] |
| CAM | 25-200 $\mu$L | 16.91 $\mu$g/mL | [16] |
| TLC | 3.75-100 $\mu$g/mL | 1.12 $\mu$g/mL | [17] |
| LC-MS/MS | 0.63-127.3 $\mu$M | 0.15 ng/mL | [18] |
| HPLC | 10-100 $\mu$g/mL | 3.6 ng/mL | [60] |
| Fluorescence | 20-100 ng/mL | 3.62 ng/mL | [61] |
| CV | 0-10 $Mdm^{-3}$ | - | [62] |
| DPV | 0.07-0.49 $\mu$g/mL | 0.2 ng/mL | **Present Work** |

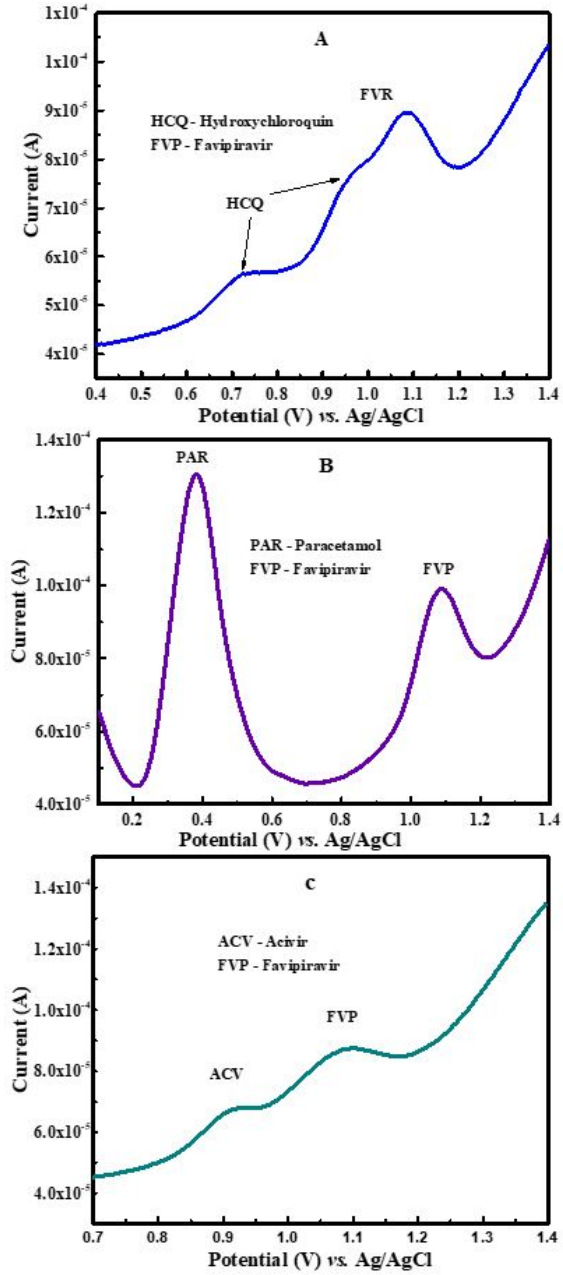


**Figure 8.** DPV curves of (A) $1.8 \times 10^{-4}$ M HCQ and FVP (B) $2.3 \times 10^{-4}$ M PAR and FAV (C) $1.6 \times 10^{-4}$ M ACV and $2 \times 10^{-5}$ MFVP at scan rate of 0.1 $Vs^{-1}$ using $G/In_2O_3$/MPGE in 0.1 M BR buffer.

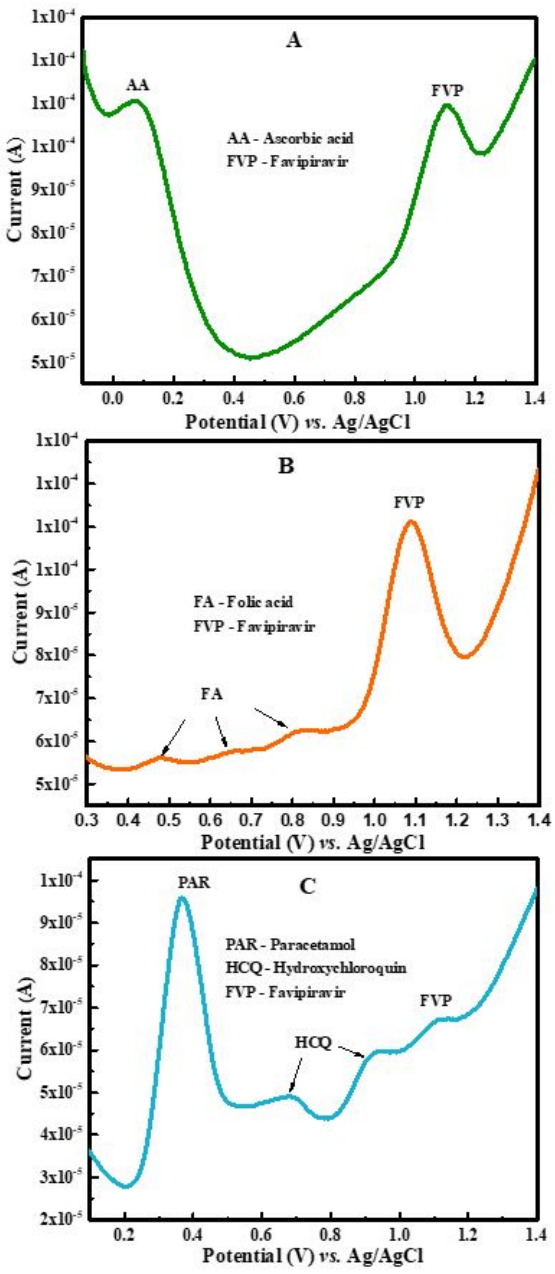


**Figure 9.** DPV plots for $2 \times 10^{-5}$ M FVP at scan rate 0.1 $Vs^{-1}$ in presence of (A) $5 \times 10^{-4}$ M AA (B) $4 \times 10^{-4}$ M FA and (C) $2.3 \times 10^{-4}$ M PAR and $1.8 \times 10^{-4}$ M HCQ.

**Table 2.** DPV analysis of FVP with and without urine sample.

| Samples | Added ($\mu$M) | Found ($\mu$M) | Recovery (%) |
|---|---|---|---|
| FVP Tablet | 3.0 | 2.85 | 95 |
| | 5.0 | 4.96 | 99 |
| In presence of urine sample | 3.0 | 2.99 | 99 |
| | 5.0 | 4.87 | 97 |

**Table 3.** Influence of interferers/tolerance limit for FVP detection by DPV.

| Excipients | EP | Standard | Tolerance Limit |
|---|---|---|---|
| HCQ | 1.081 | 1.043 | 0.0389 |
| PAR | 1.090 | 1.043 | 0.0475 |
| ACV | 0.097 | 1.043 | -0.0946 |
| AA | 1.103 | 1.043 | 0.0608 |
| FA | 1.114 | 1.043 | 0.0710 |
| PAR/HCQ | 1.108 | 1.043 | 0.0659 |

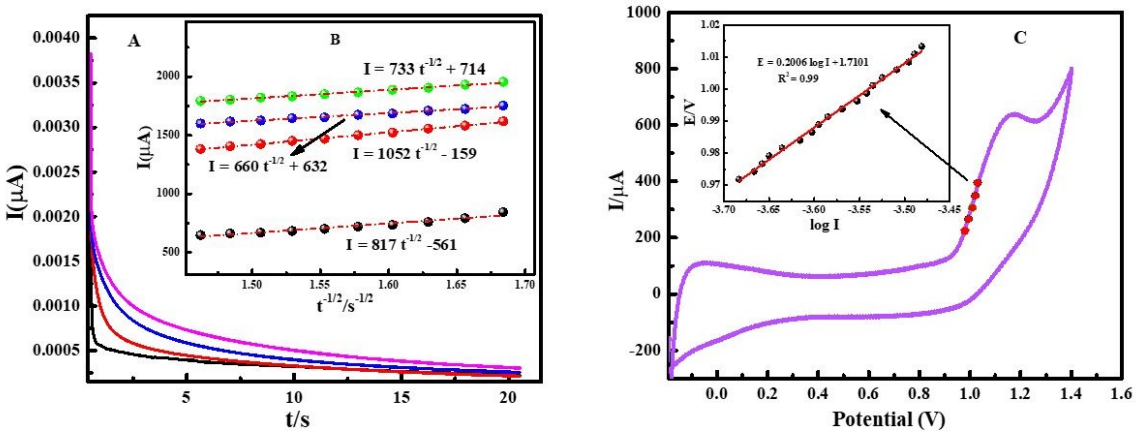


**Figure 10.** (A) Chronoamperograms for different concentrations of FVP over a period of 20 s, (B) Cottrell plots, (C) CV of 0.07 M FVP with a scan rate of 0.1 $Vs^{-1}$ and inset shows the Tafel plot (data taken from the marked region).

showed two separate oxidation peaks at 0.72 and 0.97 V with FVP 1.08 V. As shown in Fig. 8(B) Paracetamol (PAR, $2.3 \times 10^{-4}$ M) showed a high oxidation peak at 0.37 V and was well separated from FVP. At the same time, measurement of the antiviral medication Acivir (ACV) is displayed in Fig. 8(C) (ACV, $1.6 \times 10^{-4}$ M) having two well-separated peaks at 0.91 and 1.08 V with FVP. Thus, $G/In_2O_3$/MPGE provides a wide range of detection for the co-administered drugs with FVP.

Fig. 9(A) shows the detection of generally interfering substances in biological samples such as ascorbic acid (AA, vitamin C $5 \times 10^{-4}$ M), which showed anodic peak around 0.07 V. Fig. 9(B) shows detection of folic acid (FA, vitamin C $4 \times 10^{-4} M$) in presence of FVP wherein 3 oxidation peaks at 0.47 V, 0.65 V and 0.81 V were found whereas FVP was around 1.08 V. All these showed good peak current and separation from the FVP peak. Therefore, interference-free selective detection of FVP in biological samples is demonstrated. Furthermore, the simultaneous detection of PAR ($2.3 \times 10^{-4}$ M), HCQ ($2.3 \times 10^{-4}$ M), and FVP FVP could also be detected, as shown in Fig. 9(C). The PAR showed a high peak current at 0.37 V, and HCQ showed two oxidation peaks in the presence of FVP.

Therefore, we believe that the modified electrode has good detection, selectivity, and separation capacity under optimal conditions. The acceptable limit was defined as the highest concentration (4.9 $\mu$M) of FVP for which the error of detection is less than 5%. Table 3 shows the influence of interferers/tolerance limit for FVP detection by DPV.

Fig. 10(A) depicts the chronoamperometric analysis of FVP (1.4 to 5.6 $\mu$M) using $G/In_2O_3$/MPGE at 1.4 V for 20 s in 0.1 M BR buffer. The Cottrell equation is given below.

$$I = nFAC_bD^{1/2}\pi^{-1/2}t^{-1/2}$$

where $C_b$ and $D$ stand for the bulk concentration (mol $cm^{-3}$) and diffusion coefficient ($cm^2$ $s^{-1}$), respectively. Fig. 10(B) shows the Cottrell plot, which revealed the average diffusion coefficient ($D = 8.54 \times 10^{-4}$ $cm^2$ $s^{-1}$) based on the plot of Ipa vs. $t^{-1/2}$ for FVP [40]. Fig. 10(C) shows the Tafel plot and related voltage diagrams for the electro-oxidation

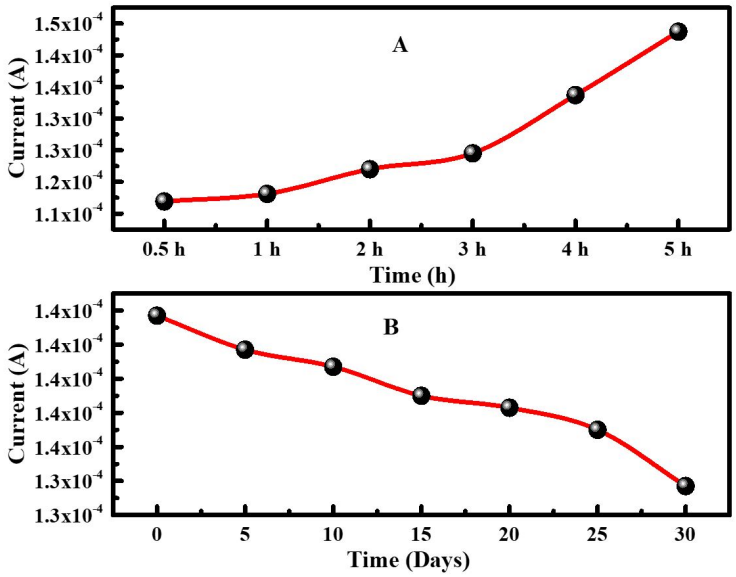


**Figure 11.** DPV current obtained for FVP (A) in hours (B) in days after fabricating the electrode in ambient condition.

of 0.07 M FVP at a 0.1 mV/s scan rate. The value of the electron transfer coefficient ($\alpha$) was found to be around 0.29 using the slope of the Tafel plot ($2.3RT/n(1-\alpha)F$). This indicates that the stimulating free energy curve for an irreversible electro-oxidation mechanism is partially symmetrical.

### 3.8 Stability and reproducibility of G/$In_2O_3$/MPGE

In order to know the stability of G/$In_2O_3$/MPGE current was measured a few hours/ days after fabricating the electrode in ambient conditions, as shown in Fig. 11(A) for 4.9 $\mu$M FVP in the 0.1 M BR buffer. The maximum current was reached after 5 h of fabricating the electrode. Hence, all the experiments were carried out in this study after keeping the electrode for 5 h in ambient conditions. However, the current was found to decrease gradually over a period of few days. Up to 30 days, around 93% of the current is retained as shown in Fig. 11(B). Hence, the electrode developed here is stable for detecting FVP, and may be employed with good precision even after several days of its fabrication. For stability (Fig. 11, F-test values for inter-day stability is 2.36% and intra-day stability is 10.61%). Further, it may be used repeatedly (4 times) as there is no significant variation of DPV current as shows (Fig. S6). Thus, G/$In_2O_3$/MPGE showed reasonable reproducibility (Fig. S6, F-test value is 4.26%). The proposed electrocatalyst is extremely sensitive to the interference-free determination of FVP in pure form, medication formulations, and in the presence of biological fluid (urine) samples. When compared to other methods listed in Table 1, G/$In_2O_3$/MPGE seems to be good in terms of stability and reproducibility [60–62].

## 4. Conclusions

In this study, $In_2O_3$ was successfully prepared towards developing a novel electrochemical sensor for an antiviral drug, FVP. The G/$In_2O_3$/MPGE alyst was fabricated and used as a working electrode for the detection of FVP (0.7 to 4.9 $\mu M$) by CV and DPV. The $R_{CT}$ of the G/$In_2O_3$/MPGE was found to be 147.6 Ω and conductivity was $1.35 \times 10^{-3}$ S $cm^{-1}$ based on Nyquist plot for $[Fe(CN)_6]^{3-/4-}$ in 0.1 M KCl solution. The G/$In_2O_3$/MPGE was used to determine pure FVP, tablet form, and in the presence of urine sample, the LOD was found to be 0.28, 0.23, and 0.30 $\mu$M, respectively. The oxidation peak for FVP is observed around 1.0 to 1.23 V in CV and DPV. In both cases, the linear behavior of Ipa vs. concentration was seen for 0.7 to 4.9 $\mu$M. The right side shift of peak current indicates the process is irreversible. The G/$In_2O_3$/MPGE showed a good response even in the presence of other co-administered drugs, HCQ, paracetamol, acivir, folic acid, and ascorbic acid. The electrode is stable for up to 30 days with a marginal decrease in anodic peak current (93% is retained). Thus, may be considered for the electro-analytical detection of important pharmaceuticals.

**Acknowledgments**

GSS greatly acknowledges RCU for sanctioning fellowship under the SC/ST grant. Authors have benefited from the facilities established under DST-FIST (SR/FST/CSI-273/2016 C), Ministry of Science and Technology, Govt. of India, and VGST-CESEM (KSTePS/VGST/CESEM/2018-19/GRD No. 746), Govt. of Karnataka, India. Dr. Naeemakhtar Momin (Sangolli Rayanna First Grade Constituent College, Belagavi) and Dr. Mohan Kumar (PES Institute of Technology and Management, Shivamogga) for their help in technical discussion.

## Supplementary Information (SI)

The characterization of G/$In_2O_3$ by powder XRD, XRD MATCH!, FTIR, TG/DSC, UV-Visible spectra, and Reproducibility for FVP (Figs. S1, S2, S3, S4, S5, and S6, respectively) are available in the supplementary information.

**Ethical Approval**

This manuscript does not report on or involve the use of any animal or human data or tissue. So the ethical approval is not applicable.

**Authors Contributions**

Authors have equally contributed in preparing the paper.

**Availability of Data and Materials**

The data that support the findings of this study are available from the corresponding author upon reasonable request.

**Conflict of Interests**

The authors declare that they have no known competing financial interests or personal relationships that could have appeared to influence the work reported in this paper.

**Open Access**

This article is licensed under a Creative Commons Attribution 4.0 International License, which permits use, sharing, adaptation, distribution and reproduction in any medium or format, as long as you give appropriate credit to the original author(s) and the source, provide a link to the Creative Commons license, and indicate if changes were made. The images or other third party material in this article are included in the article's Creative Commons license, unless indicated otherwise in a credit line to the material. If material is not included in the article's Creative Commons license and your intended use is not permitted by statutory regulation or exceeds the permitted use, you will need to obtain permission directly from the OICCPress publisher. To view a copy of this license, visit https://creativecommons.org/licenses/by/4.0.

## References

[1] K Irie, A Nakagawa, H Fujita, R Tamura, M Eto, H Ikesue, N Muroi, K Tomii, and T Hashida. "Pharmacokinetics of Favipiravir in critically Ill patients

with COVID-19.". *J. Clin. Transl. Sci.*, **13**:880–885, 2020. DOI: https://doi.org/10.1111/cts.12827.

[2] SJF Kaptein, S Jacobs, L Langendries, L Seldeslachts, S ter Horst, L Liesenborghs, B Hens, V Vergote, E Heylen, K Barthelemy, E Maas, C de Keyzer, L Bervoets, J Rymenants, T van Buyten, X Zhang, R Abdelnabi, J Pang, R Williams, HJ Thibaut, K Dallmeier, R Boudewijns, J Wouters, P Augustijns, N Verougstraete, C Cawthorne, J Breuer, C Solas, B Weynand, P Annaert, I Spriet, G Vande Velde, J Neyts, J Rocha-Pereira, and L Delang. "Favipiravir at high doses has potent antiviral activity in SARS-CoV-2-infected hamsters, whereas hydroxychloroquine lacks activity.". *PNAS*, **117**:26955–26965, 2020. DOI: https://doi.org/10.1073/pnas.2014441117.

[3] DB Shrestha, P Budhathoki, S Khadka, PB Shah, N Pokharel, and P Rashmi. "Favipiravir versus other antiviral or standard of care for COVID-19 treatment: a rapid systematic review and meta-analysis.". *Virol. J.*, **17**:141, 2020. DOI: https://doi.org/10.1186/s12985-020-01412-z.

[4] B Zhang, X Zhou, Y Qiu, Y Song, F Feng, J Feng, Q Song, Q Jia, and J Wang. "Clinical characteristics of 82 cases of death from COVID-19.". *PloS one*, **15**:7, 2020. DOI: https://doi.org/10.1371/journal.pone.0235458.

[5] MZ Tay, CM Poh, L Renia, PA MacAry, and LFP Ng. "The trinity of COVID-19: immunity, inflammation and intervention.". *Nat Rev Immunol*, **20**:363–374, 2020. DOI: https://doi.org/10.1038/s41577-020-0311-8.

[6] Y Furuta, BB Gowen, K Takahashi, K Shiraki, DF Smee, and DL Barnard. "Favipiravir (T-705), a novel viral RNA polymerase inhibitor.". *Antivir. Res.*, **100**:446–454, 2013. DOI: https://doi.org/10.1016/j.antiviral.2013.09.015.

[7] SM Megahed, AA Habib, SF Hammad, and AH Kamal. "Experimental design approach for development of spectrofluorimetric method for determination of favipiravir; a potential therapeutic agent against COVID-19 virus: Application to spiked human plasma.". *Spect. Acta. A Mol. Biomol.*, **249**:119241, 2021. DOI: https://doi.org/10.1016/j.saa.2020.119241.

[8] SJ Smither, LS Eastaugh, JA Steward, M Nelson, RP Lenk, and MS Lever. "Post-exposure efficacy of oral T-705 (Favipiravir) against inhalational Ebola virus infection in a mouse model.". *Antivir. Res.*, **104**:153–155, 2014. DOI: https://doi.org/10.1016/j.antiviral.2014.01.012.

[9] Y Furuta, T Komeno, and T Nakamura. "Favipiravir (T-705), a broad spectrum inhibitor of viral RNA polymerase.". *Proc. Jpn. Acad. Ser. B Phys. Biol. Sci.*, **93**:449–463, 2017. DOI: https://doi.org/10.2183/pjab.93.027.

[10] AA Ivashchenko, KA Dmitriev, NV Vostokova, VN Azarova, AA Blinow, AN Egorova, IG Gordeev, AP Ilin, RN Karapetian, DV Kravchenko, NV Lomakin, EA Merkulova, NA Papazova, EP Pavlikova, NP Savchuk, EN Simakina, TA Sitdekov, EA Smolyarchuk, EG Tikhomolova, EV Yakubova, and AV Ivachtchenko. "AVIFAVIR for treatment of patients with moderate Coronavirus disease 2019 (COVID-19): Interim results of a phase II/III multicenter randomized clinical trial.". *Clin. Infect. Dis.*, **73**:531–534, 2021. DOI: https://doi.org/10.1093/cid/ciaa1176.

[11] M Ghasemnejad-Berenji and S Pashapour. "Favipiravir and COVID-19: A simplified summary". *Drug Res.*, **71**:166–170, 2020. DOI: https://doi.org/10.1055/a-1296-7935.

[12] Y Lou, L Liu, H Yao, X Hu, J Su, K Xu, R Luo, X Yang, L He, X Lu, Q Zhao, T Liang, and Y Qiu. "Clinical outcomes and plasma concentrations of baloxavir Marboxil and Favipiravir in COVID-19 patients: An exploratory randomized, controlled trial.". *Eur. J. Pharm. Sci.*, **157**:105631, 2021. DOI: https://doi.org/10.1016/j.ejps.2020.105631.

[13] K Shiraki and T Daikoku. "Favipiravir, an anti-influenza drug against life-threatening RNA virus infections.". *Pharmacol. Ther.*, **209**:107512, 2020. DOI: https://doi.org/10.1016/j.pharmthera.2020.107512.

[14] V Pilkington, T Pepperrell, and A Hill. "A review of the safety of favipiravir - a potential treatment in the COVID-19 pandemic?". *J. Virus Erad.*, **6**:45–51, 2020. DOI: https://doi.org/10.1016/S2055-6640(20)30016-9.

[15] I Bulduk. "HPLC-UV method for quantification of favipiravir in pharmaceutical formulations.". *Acta. Chromat.*, **33**:209–215, 2021. DOI: https://doi.org/10.1556/1326.2020.00828.

[16] Y Moriiwa, N Oyama, R Otsuka, K Morioka, A Shoji, and A Yanagida. "Development of a colorimetric assay for quantification of favipiravir in human serum using ferrihydrite.". *Talanta*, **252**:123827, 2023. DOI: https://doi.org/10.1016/j.talanta.2022.123827.

[17] RE Saraya, S Deeb El, BI Salman, and AE Ibrahim. "Highly sensitive high-performance thin-layer chromatography method for the simultaneous determination of molnupiravir, favipiravir, and ritonavir in pure forms and pharmaceutical formulations.". *J. Sep. Sci.*, **45**:2582–2590, 2022. DOI: https://doi.org/10.1002/jssc.202200178.

[18] MI Morsy, EG Nouman, YM Abdallah, MA Zainelabdeen, MM Darwish, AY Hassan, AS Gouda, MR Rezk, AM Abdel-Megied, and HM Marzouk. "A novel LC-MS/MS method for determination of the potential antiviral candidate favipiravir for the emergency treatment of SARS-CoV-2

virus in human plasma: Application to a bioequivalence study in Egyptian human volunteers.". *J. Pharm. Biomed. Anal.*, **199**:114057, 2021. DOI: https://doi.org/10.1016/j.jpba.2021.114057.

[19] VD Hoang and NT Yen. "Adsorptive cathodic stripping voltammetric determination of cefoperazone in bulk powder, pharmaceutical dosage forms, and human urine.". *J. Anal. Chem*, **12**:783–790, 2013. DOI: https://doi.org/10.1155/2013/367914.

[20] AT Chipeture, D Apath, and M Moyo. "Multiwalled carbon nanotubes decorated with bismuth (III) oxide for electrochemical detection of an antipyretic and analgesic drug paracetamol in biological samples". *J. Anal. Sci. Technol.*, **10**:22, 2019. DOI: https://doi.org/10.1186/s40543-019-0181-5.

[21] L Ahmadpour-Mobarakeh and A Nezamzadeh-Ejhieh. "A zeolite modified carbon paste electrode as useful sensor for voltammetric determination of acetaminophen.". *Mater. Sci. Eng. C.*, **49**:493–499, 2019. DOI: https://doi.org/10.1016/j.msec.2015.01.028.

[22] H Kumar and B Gupta. "Development of novel electrochemical sensor for the detection of biological warfare agents: enzyme, antibody, and DNA free.". *SN. Appl. Sci.*, **2**:1957, 2020. DOI: https://doi.org/10.1007/s42452-020-03706-x.

[23] FS Omar, N Duraisamy, K Ramesh, and S Ramesh. "Conducting polymer and its composite materials based electrochemical sensor for Nicotinamide Adenine Dinucleotide (NADH).". *Biosens. and Bioelectron*, **79**:763–775, 2016. DOI: https://doi.org/10.1016/j.bios.2016.01.013.

[24] MHF Taha, H Ashraf, and W Caesarendra. "A brief description of cyclic voltammetry transducer-based non-enzymatic glucose biosensor using synthesized graphene electrodes.". *Appl. Syst. Innov.*, **3**:1–32, 2020. DOI: https://doi.org/10.3390/asi3030032.

[25] X Xu, T Wu, F Xia, Y Li, C Zhang, L Zhang, M Chen, X Li, L Zhang, Y Liu, and J Gao. "Redox reaction between graphene oxide and In powder to prepare $In_2O_3$/reduced graphene oxide hybrids for supercapacitors.". *J. Power Sources*, **266**:282–290, 2014. DOI: https://doi.org/10.1016/j.jpowsour.2014.05.051.

[26] RR Sawkar, MM Shanbhag, SM Tuwar, K Mondal, and NP Shetti. "Sodium dodecyl sulfate–mediated graphene sensor for electrochemical detection of the antibiotic drug: ciprofloxacin.". *Materials*, **15**:7872, 2020. DOI: https://doi.org/10.3390/ma15227872.

[27] S Meenakshi, S Jancy Sophia, and K Pandian. "High surface graphene nanoflakes as sensitive sensing platform for simultaneous electrochemical detection of metronidazole and chloramphenicol.". *Mater. Sci. Eng. C.*, **90**:407–419, 2018. DOI: https://doi.org/10.1016/j.msec.2018.04.064.

[28] L Gao, C Lian, Y Zhou, L Yan, Q Li, C Zhang, L Chen, and K Chen. "Graphene oxide-DNA based sensors.". *Biosens. and Bioelectron.*, **60**:22–29, 2014. DOI: https://doi.org/10.1016/j.bios.2014.03.039.

[29] FFN Tuzluca, YO Yesilbag, and M Ertugrul. "Synthesis of $In_2O_3$ nanostructures with different morphologies as potential supercapacitor electrode materials.". *Appl. Surf. Scie.*, **427**:956–964, 2018. DOI: https://doi.org/10.1016/j.apsusc.2017.08.127.

[30] B Li, Y Xie, M Jing, G Rong, Y Tang, and G Zhang. "$In_2O_3$ hollow microspheres: Synthesis from designed $In(OH)_3$ precursors and applications in gas sensors and photocatalysis.". *Langmuir*, **22**:9380–9385, 2006. DOI: https://doi.org/10.1021/la061844k.

[31] X Liang, G Jin, F Liu, X Zhang, S An, J Ma, and G Lu. "Synthesis of $In_2O_3$ hollow nanofibers and their application in highly sensitive detection of acetone.". *Ceram. Int.*, **41**:13780–13787, 2015. DOI: https://doi.org/10.1016/j.ceramint.2015.08.060.

[32] X Xu, X Mei, P Zhao, P Sun, Y Sun, X Hu, and G Lu. "One-step synthesis and gas sensing characteristics of urchin-like $In_2O_3$.". *Sens. and Actu, B: Chem.*, **186**:61–66, 2013. DOI: https://doi.org/10.1016/j.snb.2013.05.029.

[33] Z Yang, X Huang, R Zhang, J Li, Q Xu, and X Hu. "Novel urchin-like $In_2O_3$–chitosan modified electrode for direct electrochemistry of glucose oxidase and biosensing.". *Electrochim. Acta.*, **70**:325–330, 2012. DOI: https://doi.org/10.1016/j.electacta.2012.03.075.

[34] M Mansha, A Qurashi, N Ullah, FO Bakare, I Khan, and ZH Yamani. "Synthesis of $In_2O_3$/graphene heterostructure and their hydrogen gas sensing properties.". *Ceram. Int.*, **42**:11490–11495, 2016. DOI: https://doi.org/10.1016/j.ceramint.2016.04.035.

[35] N Singh, A Ponzoni, E Comini, and PS Lee. "Chemical sensing investigations onZn-$In_2O_3$ nanowires.". *Sens. Actuators B: Chem.*, **171-172**:244–248, 2012. DOI: https://doi.org/10.1016/j.snb.2012.03.054.

[36] J Wang, B Zou, S Ruan, J Zhao, and F Wu. "Synthesis, characterization, and gas-sensing property for HCHO of Ag-doped $In_2O_3$ nanocrystalline powders.". *Mater. Chem. Phys.*, **117**:489–493, 2009. DOI: https://doi.org/10.1016/j.matchemphys.2009.06.045.

[37] Q Huang, Y Cao, Y Chen, W Huang, X Wang, K Zhang, and J Tu. "Mesoporous indium oxide for nonenzymatic uric acid sensing.". *Int. Proc. Chem. Biol. Environ. Eng.*, **10**:69–72, 2015. DOI: https://doi.org/10.2991/mebe-15.2015.17.

[38] D Chu, J Wang, S Wang, L Zha, J He, Y Hou, Y Yan, H Lin, and Z Tian. "High activity of Pd-$In_2O_3$/CNTs electrocatalyst for electro-oxidation of ethanol.". *Catal. Commun.*, **10**:955–958, 2009. DOI: https://doi.org/10.1016/j.catcom.2008.12.041.

[39] S Allahverdiyeva, O Yunusoğlu, Y Yardım, and Z Şentürk. "First electrochemical evaluation of favipiravir used as an antiviral option in the treatment of COVID-19: A study of its enhanced voltammetric determination in cationic surfactant media using a boron-doped diamond electrode.". *Anal. Chim. Acta.*, **1159**:338418, 2021. DOI: https://doi.org/10.1016/j.aca.2021.338418.

[40] M Mehmandoust, Y Khoshnavaz, M Tuzen, and N Erk. "Voltammetric sensor based on bimetallic nanocomposite for determination of favipiravir as an antiviral drug.". *Microchim. Acta.*, **188**:434, 2021. DOI: https://doi.org/10.1007/s00604-021-05107-2.

[41] J Lee, P Dak, Y Lee, H Park, W Choi, MA Alam, and S Kim. "Two-dimensional layered $MoS_2$ biosensors enable highly sensitive detection of biomolecules.". *Sci. Rep.*, **4**:7352, 2014. DOI: https://doi.org/10.1038/srep07352.

[42] SM Saleh, R Ali, F Alminderej, and IAI Ali. "Ultrasensitive optical chemosensor for Cu(II) detection.". *Int. J. Anal. Chem.*, **2019**:8, 2019. DOI: https://doi.org/10.1155/2019/7381046.

[43] SC Kulkarni and DS Patil. "Synthesis and characterization of uniform spherical shape nanoparticles of indium oxide.". *J. Mater. Sci. Mater. Electron*, **27**:3731–3735, 2016. DOI: https://doi.org/10.1007/s10854-015-4215-5.

[44] A Shanmugasundaram, V Gundimeda, T Hou, and DW Lee. "Realizing synergy between $In_2O_3$ nanocubes and nitrogen-doped reduced graphene oxide: An excellent nanocomposite for the selective and sensitive detection of CO at ambient temperatures.". *ACS Appl. Mater. Interfaces*, **9**:31728–31740, 2017. DOI: https://doi.org/10.1021/acsami.7b06253.

[45] P Gogoi, S Hazarika, and P Barman. "Role of TBATB in nano indium oxide catalyzed C-S bond formation.". *Sci. Rep.*, **5**:13873, 2015. DOI: https://doi.org/10.1038/srep13873.

[46] ND Chinh, ND Quang, H Lee, TT Hien, NM Hieu, D Kim, C Kim, and D Kim. "NO gas sensing kinetics at room temperature under UV light irradiation of $In_2O_3$ nanostructures.". *Sci. Rep.*, **6**:35066, 2016. DOI: https://doi.org/10.1038/srep35066.

[47] J Xu and X Wang. "Hydrothermal synthesis of $In_2O_3$ for detecting $H_2S$ in air.". *Sens. and Actu. B: Chem.*, **115**:642–646, 2006. DOI: https://doi.org/10.1016/j.snb.2005.10.038.

[48] Ö Göktuğ, E Altaş, G Kayar, and M Gökalp. "The development and the validation of a novel dissolution method of favipiravir film-coated tablets.". *Sci. Pharm.*, **90**:3, 2021. DOI: https://doi.org/10.3390/scipharm90010003.

[49] JB Jyothi and VR Kavya. "Ultraviolet spectrophotometric method development for estimation of new antiviral repurposing drug favipiravir.". *AJPCR*, **14**:67–69, 2021. DOI: https://doi.org/10.22159/ajpcr.2021.v14i7.41966.

[50] CY Hsu, KM Lee, JH Huang, KR Justin Thomas, JT Lin, and KC Ho. "A novel photoelectrochromic device with dual application based on poly(3,4-alkylenedioxythiophene) thin film and an organic dye.". *J. Power Sources*, **185**:1505–1508, 2008. DOI: https://doi.org/10.1016/j.jpowsour.2008.09.031.

[51] M Nosuhi and A Nezamzadeh-Ejhieh. "An indirect application aspect of zeolite modified electrodes for voltammetric determination of iodate.". *J. Electroanal. Chem.*, **810**:119–128, 2018. DOI: https://doi.org/10.1016/j.jelechem.2017.12.075.

[52] Z Amani-Beni and A Nezamzadeh-Ejhieh. "NiO nanoparticles modified carbon paste electrode as a novel sulfasalazine sensor.". *Ana. Chim. Acta.*, **1031**:47–59, 2018. DOI: https://doi.org/10.1016/j.aca.2018.06.002.

[53] M Srivastava, P Tiwari, VK Mall, SK Srivastava, and R Prakash. "Voltammetric determination of the antimalarial drug chloroquine using a glassy carbon electrode modified with reduced graphene oxide on $WS_2$ quantum dots.". *Microchim. Acta*, **186**:415, 2019. DOI: https://doi.org/10.1007/s00604-019-3525-3.

[54] S Yan-mei, C Li-qin, L Mei, C Zhi-hong, L Xiu-min, and M Ming-san. "Soluble tetraaminophthalocyanines indium functionalized graphene platforms for rapid and ultra-sensitive determination of rutin in Tartary buckwheat tea.". *Food Cont.*, **132**:108550, 2022. DOI: https://doi.org/10.1016/j.foodcont.2021.108550.

[55] A Ahmadi and A Nezamzadeh-Ejhieh. "A comprehensive study on electrocatalytic current of urea oxidation by modified carbon paste electrode with Ni(II)-clinoptilolite nanoparticles: Experimental design by response surface methodology.". *J. Electroanal. Chem.*, **801**:328–337, 2017. DOI: https://doi.org/10.1016/j.jelechem.2017.08.009.

[56] MH Sheikh-Mohseni and A Nezamzadeh-Ejhieh. "Modification of carbon paste electrode with Ni-clinoptilolite nanoparticles for electrocatalytic oxidation of methanol.". *Electrochim. Acta.*, **147**:572–581, 2014. DOI: https://doi.org/10.1016/j.electacta.2014.09.123.

[57] K Prabhu, SJ Malode, RM Kulkarni, and NP Shetti. "Improved electrochemical detection of harmful 1-NAA molecules by a MWNTs/Ca-ZnO nanocomposite-modified paste electrode.". *New J. Chem.*, **47**:315–323, 2022. DOI: https://doi.org/10.1039/D2NJ05060A.

[58] A Mehrabi, M Rahimnejad, M Mohammadi, and M Pourali. "Electrochemical detection of Flutamide as an anticancer drug with gold nanoparticles modified glassy carbon electrode in the presence of prostate cancer cells.". *J. Appl. Electrochem.*, **51**:597–606, 2021. DOI: https://doi.org/10.1007/s10800-020-01519-9.

[59] P Balasubramanian, TST Balamurugan, S-M Chen, T-W Chen, G Sharmila, and M Yu. "One-step green synthesis of colloidal gold nano particles: A potential electrocatalyst towards high sensitive electrochemical detection of methyl parathion in food samples.". *J. Taiwan Inst. Chem. Eng.*, **87**:83–90, 2018. DOI: https://doi.org/10.1016/j.jtice.2018.03.014.

[60] IE Mikhail, H Elmansi, F Belal, and A Ehab. "Green micellar solvent-free HPLC and spectrofluorimetric determination of favipiravir as one of COVID-19 antiviral regimens.". *J. Microchem.*, **165**:106189, 2021. DOI: https://doi.org/10.1016/j.microc.2021.106189.

[61] I Hazarika, T Kalita, P Deka, SK Gogoi, K Althubeiti, R Thakuria, and B Gogoi. "Soot-based reduced graphene quantum dot/hemin conjugate for favipiravir sensing.". *ACS Appl. Nano Mater.*, **4**:13927–13937, 2021. DOI: https://doi.org/10.1021/acsanm.1c03235.

[62] T Nakayama and R Honda. "Electrochemical and mechanistic study of oxidative degradation of favipiravir by electrogenerated superoxide through proton-coupled electron transfer.". *ACS Omega*, **6**:21730–21740, 2021. DOI: https://doi.org/10.1021/acsomega.1c03230.